energies

Article

A New Approach for the Measurement of the Complex Value of Fault-Loop Impedance in Low-Voltage Electrical Installations

Grzegorz Hołdyński , Zbigniew Skibko and Wojciech Walendziuk *

Faculty of Electrical Engineering, Bialystok University of Technology, Wiejska 45D, 15-351 Bialystok, Poland; g.holdynski@pb.edu.pl (G.H.); z.skibko@pb.edu.pl (Z.S.)
* Correspondence: w.walendziuk@pb.edu.pl

Abstract

The primary method for verifying the safety of electrical installations is the measurement of fault-loop impedance. The most common approach involves measuring the voltage under no-load and load conditions and determining the difference between them. However, this method has several drawbacks, including the need for complex instrumentation and measurement uncertainty that depends on the magnitude and nature of the load in the tested electrical system. Additionally, most existing measurement systems allow only the determination of the impedance modulus. This paper introduces a novel, theoretically grounded method for measuring fault-loop impedance. The proposed approach is based on measuring the RMS no-load voltage, followed by three voltage measurements under different loading conditions using reference impedances with known phase angles (defined by the resistance-to-reactance ratio). The complex value of the fault-loop impedance is then obtained using a second-degree polynomial approximation. The main advantage of the proposed method is that it reduces the influence of slowly varying operating loads under quasi-stationary network conditions of the network on measurement accuracy. This property requires experimental verification. It should be noted that the presented analysis is of a theoretical nature and constitutes a basis for further research and discussion within the scientific community.

Keywords: fault-loop impedance; complex impedance; polynomial approximation; electric shock protection

1. Introduction

The measurement of fault-loop impedance is one of the basic methods used to verify the safety of low-voltage electrical installations [1–3]. The knowledge of the value of this quantity enables verification of protection conditions in the event of a short circuit in the system [4]. Protection by automatic disconnection of supply is adequate when the protective device automatically switches off the power supply within the required time, and the regulatory permissible touch voltage values are not exceeded [5,6]. The automatic disconnection time in systems with effective switch-off TN (for 230 V) is 0.4 s in consumer circuits and a maximum of 5 s in distribution circuits [6,7]. In a TN network, in order to check the effectiveness of the anti-shock protection by automatic disconnection of supply, it should be determined whether the value of the fault-loop impedance meets the following condition [1,8]:

$$Z_S \leq \frac{U_0}{I_a}, \tag{1}$$

Received: 8 June 2026
Revised: 27 July 2026
Accepted: 4 August 2026
Published: 6 August 2026

where Z_s is the fault-loop impedance of the circuit under test, I_a is the protection current causing the power supply to be switched off within the required time, U_0 is the rated voltage of the network to earth.

Fault-loop impedance measurement is also widely used to analyze and predict the resonance and stability of the power system with connected inverters [9–12]. Modern grid-impedance estimation methods are primarily intended for online monitoring and stability assessment at the point of connection of power-electronic converters. These methods generally require simultaneous voltage and current measurements and have a different application objective from fault-loop impedance testing in low-voltage installations. Therefore, the classical voltage-drop method was selected as the most directly comparable reference method in the present study. Impedance values are also used to assess the power quality of electricity [13], to identify transmission line parameters [14], and to assess the condition of power transformer windings [15,16]. There are two main methods for measuring fault-loop impedance. The first, indirect, method is based on a technical method in which the resistance R_x and reactance X_x values must be measured separately for the fault-loop under test. This method is characterized by the complexity of the measurements and the large size of the measuring instruments. An extension of this measurement method is the use of a resistive-reactance load. The main disadvantage of this method is the time-consuming nature of the measurements, which require at least three readings across different resistance and reactance values. The sought value of the fault-loop impedance Z_S is then the geometric sum of the measured values [17]:

$$Z_S \leq \sqrt{R_X^2 + X_X^2}. \tag{2}$$

When measuring the fault-loop impedance, there is a risk of dangerous touch voltages appearing on accessible conductive parts, which is the reason why the method is very rarely used.

The second, direct, method is the measurement of the fault-loop impedance using an 'artificial short circuit' (voltage drop) method [18]. It is currently the most common method for determining the fault-loop impedance value [19]. The impedance is determined by the measurement of the voltage value U_1 before the load with known impedance Z_0 is switched on and the voltage U_2 after it is switched on [20,21]:

$$Z_S = Z_0 \frac{U_1 - U_2}{U_2} = Z_0 \left(\frac{U_1}{U_2} - 1 \right), \tag{3}$$

where Z_S—measured impedance, Z_0—measurement load impedance, U_1—voltage measured before the measurement load is switched on, U_2—voltage measured after the measurement load is switched on.

The choice of instruments for direct measurement of short-circuit loops is wide. The measurement methodology has been described in mathematical detail, and the physical phenomena accompanying it have been described in [2,22–24]. The disadvantage of this solution is primarily the variable measurement error, which depends on the measured impedance value. This method is modified to measure and compare the voltage between the phase conductor and the protective conductor (with the measurement load switched on or off). Another method of direct measurement of the fault-loop impedance short-circuit consists of measuring the value of the instantaneous voltage at time t and $(t + T)/2h$ (where T is the period of the supply voltage waveform, h—the harmonic order) with the measurement load switched off, from which sums are formed, being the orthogonal component of the voltage in the unloaded state [25–27]. The number of measurement repetitions is in accordance with the number of harmonics eliminated. A common disadvantage of this type of solution is the complexity of the measurement systems and the measurement uncertainty strictly dependent on the degree and nature of the load in the electrical system under test [4,7].

An extension of the direct measurement methods for fault-loop impedance, proposed by the authors, consists of measuring the RMS value of the test network voltage: in one period, the test circuit is loaded with the measurement current, and in the second period, the system is left unloaded. The desired value of the fault-loop impedance is obtained using quadratic polynomial approximation. A potential feature of the proposed method is its reduced sensitivity to slowly varying network loads, provided that the voltage-stationarity criterion is satisfied.

Objective and Contributions of the Paper

The main objective of this study is to develop a measurement method and a dedicated circuit to determine the complex impedance of the fault loop in low-voltage electrical installations (rated voltage ≤ 1 kV). The proposed solution supports the assessment of the effectiveness of electric shock protection implemented through automatic power disconnection. Unlike previous techniques, the presented method enables automatic impedance estimation and, according to this theoretical analysis, can reduce sensitivity to slowly changing network load conditions. The scope of work includes:

- unlike existing methods, the proposed approach allows for direct estimation of complex impedance without the need for phase measurement, relying solely on RMS voltage measurements and polynomial approximation;
- formulation of an algorithm for calculating the complex fault-loop impedance using three defined measurement impedances and a second-degree polynomial model;
- reduction in the structural complexity and size of measurement systems through the use of electronically controlled measurement branches and full automation of the measurement sequence;
- improvement of measurement reliability by eliminating the influence of variable network loads and utilizing measurements of effective voltage values in loaded and unloaded states;
- design of a measurement uncertainty estimation based on an analytical approach supported by Monte Carlo analysis.

To confirm the effectiveness of the proposed solution, theoretical analyses and simulation-based studies were conducted to evaluate the accuracy of the proposed method and its uncertainty characteristics. It is worth stressing that the present study is limited to TN low-voltage installations, which constitute the primary application area of fault-loop impedance measurements. In the case of TT and IT systems, measuring fault-loop impedance does not confirm the effectiveness of electric shock protection.

2. Materials and Methods

The authors propose a method based on RMS voltage analysis to measure complex fault-loop impedance [28]. The procedure involves cycling the load and unloading the circuit while measuring the current to determine the short-circuit impedance (Figure 1).

In the first step, the RMS voltage of the low-voltage network (E_{11}) is measured over one full period (see Figure 2). In the next step, a test circuit containing three reference impedances (Z_{p1}, Z_{p2}, Z_{p3}), with known modulus and phase values, is connected to the circuit. After connecting the first measurement branch with impedance Z_{p1} and waiting for a stabilization time t_1 (to let transient states settle), the RMS value of the voltage U_{p1} is measured. The times t_1 and t_2 are identical for all sequences, respectively.

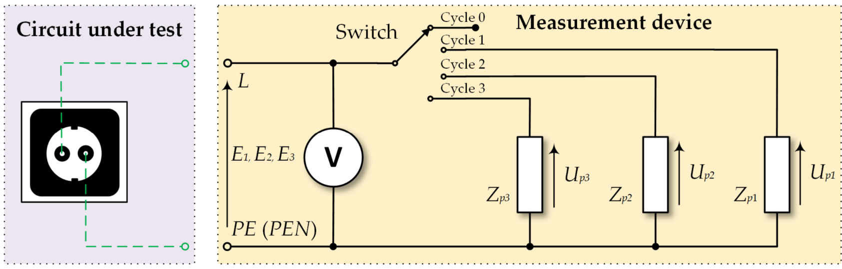

Figure 1. Diagram illustrating the concept behind the proposed method for measuring a fault-loop impedance.

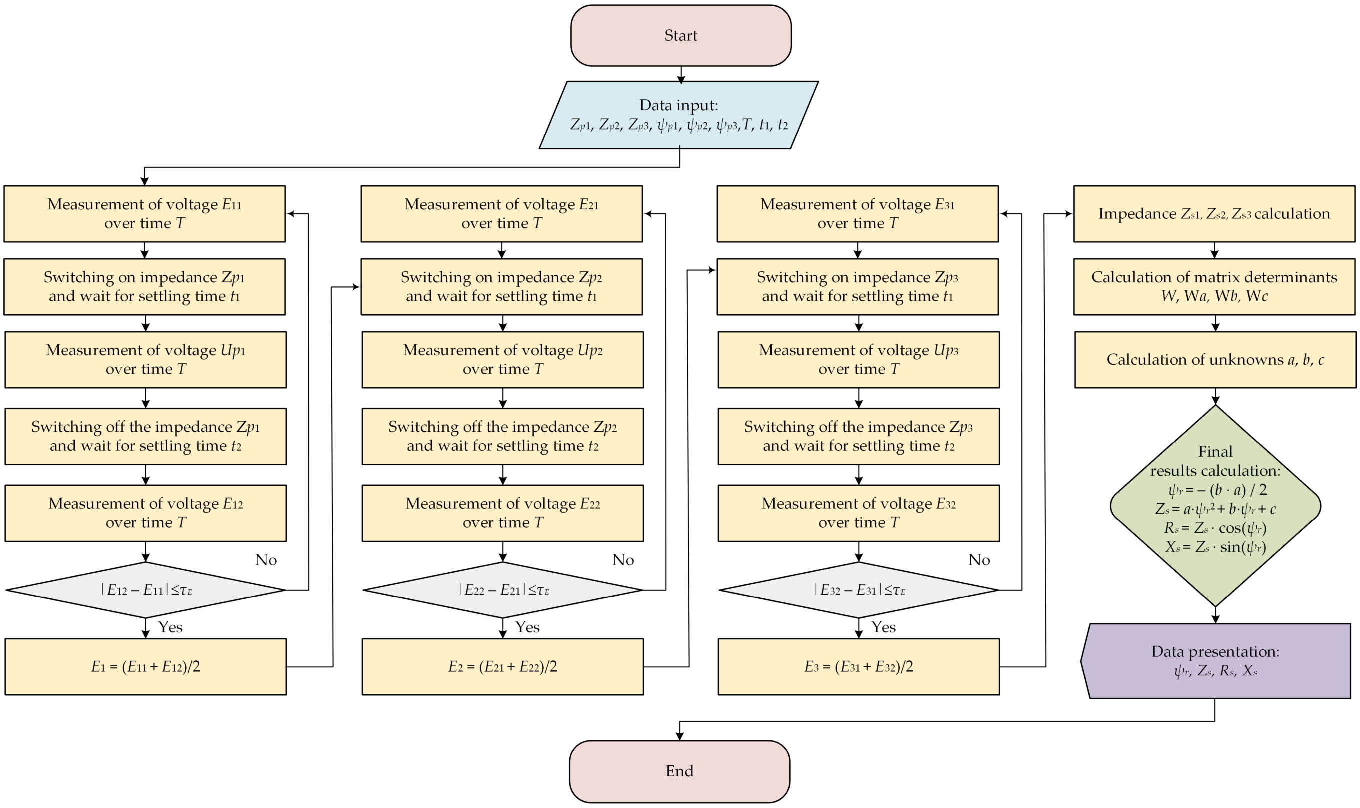

Figure 2. Flowchart of the proposed algorithm for fault-loop impedance measurement.

After a time interval T (where T is the period of the tested network voltage), the first impedance is disconnected, and after the stabilization time t_1, the network voltage (E_{12}) is measured again. If $|E_{12} - E_{11}| > \tau_E$, where τ_E is the acceptance threshold determined from the voltage-measurement uncertainty and permissible short-term supply-voltage variations, the measurement is repeated from the beginning. Otherwise, the RMS voltage U_{p1} is recorded, and the representative unloaded voltage is calculated as $E_1 = (E_{11} + E_{12})/2$.

Next, the second measurement branch with impedance Z_{p2} is activated, and after time t_1, the RMS value of the voltage U_{p2} is measured. After measurement time T, the second impedance is disconnected, and after t_1, the network voltage (E_{22}) is measured again. If $|E_{22} - E_{21}| > \tau_E$, the measurement is repeated from the beginning of this stage. Otherwise, the RMS voltage U_{p2} is recorded, the representative unloaded voltage is calculated as $E_2 = (E_{21} + E_{22})/2$, and the third measurement branch with impedance $\underline{Z}_{p3}$ is activated. After stabilization time t_1, the RMS value of the voltage U_{p3} is measured. After time T, the third impedance is disconnected. If $|E_{32} - E_{31}| > \tau_E$, the measurement for the third reference impedance is repeated from the beginning of this stage. Otherwise, the RMS voltage U_{p3} is recorded, and the representative unloaded voltage is calculated as

$E_3 = (E_{31} + E_{32})/2$. It is worth noting that in practical implementations, the switching of the three reference impedances can be performed using semiconductor switches controlled by a microcontroller. This allows the measurement process, stabilization periods, RMS calculations, polynomial approximation, and displaying results to be fully automated within a dedicated digital measuring device.

In the 230 V network under consideration, the three reference branches draw currents of approximately 4.58 A, 4.59 A, and 4.62 A, which correspond to apparent powers of approximately 1.05 kVA. Since each branch is powered only during the stabilization period and the measurement of the voltage rms value, the reference components must be selected based on their permissible short-time current rather than their continuous current. Electronic switches must be rated for line voltage, peak current, and transient overvoltages. Inductive branches additionally require controlled switching and protection against switching overvoltages. The stabilization time must be determined experimentally to ensure sufficient decay of transient components. The total measurement time includes three measurement intervals: voltage under load and without load, stabilization delays, and switching times. A practical device should also include galvanic isolation, overcurrent and overheating protection, safe discharge paths, and protection against hazardous touch voltages. These aspects will be verified experimentally in future work.

Based on the obtained RMS values of the tested network voltages (E_1, E_2, E_3) and the measured voltages (U_{p1}, U_{p2}, U_{p3}) for the respective measurement branches, the fault-loop impedance modulus values Z_{si} (where i = 1, 2, 3 denotes the measurement branch number) are calculated. A second-degree polynomial is used for these calculations, allowing precise determination of the complex impedance value of the tested short-circuit loop.

$$Z_{si} = Z_{pi} \cdot \frac{E_i - U_{pi}}{U_{pi}}, \quad i = 1,\ 2,\ 3 \tag{4}$$

The relationship between the fault-loop impedance modulus (Z_{si}) and the measurement impedance (angle $\psi_{(p)(i)}$) can be described by a second-degree polynomial:

$$Z_{si}(\psi_{pi}) = a \cdot \psi_{pi}^2 + b \cdot \psi_{pi} + c. \tag{5}$$

The coefficients a, b, and c of the polynomial (5) are determined for the three measurement points by solving the following system of equations:

$$\begin{cases} {\psi^2}_{p1} \cdot a \ + \ \psi_{p1} \cdot b \ + \ c \ = \ Z_{s1} \\ {\psi^2}_{p2} \cdot a \ + \ \psi_{p2} \cdot b \ + \ c \ = \ Z_{s2} \\ {\psi^2}_{p3} \cdot a \ + \ \psi_{p3} \cdot b \ + \ c \ = \ Z_{s3} \end{cases} \tag{6}$$

Since three unknown polynomial coefficients (a, b, and c) must be determined, at least three independent measurement points are required. Therefore, the proposed method employs three reference impedances with different phase angles, providing a unique solution of the system of equations. Then using Cramer's method, the determinants of the system coefficient matrix are obtained:

$$W = \begin{vmatrix} \psi_{p1}^2 & \psi_{p1} & 1 \\ \psi_{p2}^2 & \psi_{p2} & 1 \\ \psi_{p3}^2 & \psi_{p3} & 1 \end{vmatrix} \tag{7}$$

$$W_a = \begin{vmatrix} Z_{s1} & \psi_{p1} & 1 \\ Z_{s2} & \psi_{p2} & 1 \\ Z_{s3} & \psi_{p3} & 1 \end{vmatrix} \tag{8}$$

https://doi.org/10.3390/en19153695

$$W_b = \begin{vmatrix} \psi_{p1}^2 & Z_{s1} & 1 \\ \psi_{p2}^2 & Z_{s2} & 1 \\ \psi_{p3}^2 & Z_{s3} & 1 \end{vmatrix} \tag{9}$$

$$W_c = \begin{vmatrix} \psi_{p1}^2 & \psi_{p1} & Z_{s1} \\ \psi_{p2}^2 & \psi_{p2} & Z_{s2} \\ \psi_{p3}^2 & \psi_{p3} & Z_{s3} \end{vmatrix} \tag{10}$$

and then the values of the coefficients of the polynomial:

$$a = \frac{W_a}{W} \qquad b = \frac{W_b}{W} \qquad c = \frac{W_c}{W} \tag{11}$$

$$\begin{aligned} a &= \frac{Z_{s1}\psi_{p2} - Z_{s1}\psi_{p3} - Z_{s2}\psi_{p1} + Z_{s2}\psi_{p3} + Z_{s3}\psi_{p1} - Z_{s3}\psi_{p2}}{\psi_{p1}^2\psi_{p2} - \psi_{p1}^2\psi_{p3} - \psi_{p1}\psi_{p2}^2 + \psi_{p1}\psi_{p3}^2 + \psi_{p2}^2\psi_{p3} - \psi_{p2}\psi_{p3}^2} \\ b &= \frac{-Z_{s1}\psi_{p2}^2 + Z_{s1}\psi_{p3}^2 + Z_{s2}\psi_{p1}^2 - Z_{s2}\psi_{p3}^2 - Z_{s3}\psi_{p1}^2 + Z_{s3}\psi_{p2}^2}{\psi_{p1}^2\psi_{p2} - \psi_{p1}^2\psi_{p3} - \psi_{p1}\psi_{p2}^2 + \psi_{p1}\psi_{p3}^2 + \psi_{p2}^2\psi_{p3} - \psi_{p2}\psi_{p3}^2} \\ c &= \frac{Z_{s1}\psi_{p2}^2\psi_{p3} - Z_{s1}\psi_{p2}\psi_{p3}^2 - Z_{s2}\psi_{p1}^2\psi_{p3} + Z_{s2}\psi_{p1}\psi_{p3}^2 + Z_{s3}\psi_{p1}^2\psi_{p2} - Z_{s3}\psi_{p1}\psi_{p2}^2}{\psi_{p1}^2\psi_{p2} - \psi_{p1}^2\psi_{p3} - \psi_{p1}\psi_{p2}^2 + \psi_{p1}\psi_{p3}^2 + \psi_{p2}^2\psi_{p3} - \psi_{p2}\psi_{p3}^2} \end{aligned} \tag{12}$$

It is worth noting that Equation (11) presents the general form of the solution obtained using Cramer's rule, whereas Equation (12) provides the corresponding explicit analytical expressions after expanding the determinants.

For $\underline{Z}_s = Z_s e^{j\psi_s}$ and $\underline{Z}_p = Z_p e^{j\psi_p}$, the value determined from the measured voltage drop reaches its maximum when the phase angles of both impedances are equal, i.e., when $\psi_p = \psi_s$. At this point, the maximum value corresponds to the fault-loop impedance modulus Z_s, whereas the position of the maximum determines its phase angle ψ_s. The second-degree polynomial is therefore used as a three-point approximation of this relationship. The solution is considered physically valid only when $a < 0$ and $0° \leq -b/(2a) \leq 90°$. If these conditions are not satisfied, the complex impedance estimate is rejected.

In light of the above, the desired, actual value of the fault-loop impedance modulus of the circuit under test is the maximum of the function (Z_s) $Z_{s(i)}(\psi_{p(i)})$. The argument (ψ_r) at which the maximum of the function occurs, $Z_{s(i)}(\psi_{p(i)})$ is the actual angle of the fault-loop impedance:

$$\psi_r = \frac{-b}{2a}. \tag{13}$$

The actual value of the fault-loop impedance modulus (Z_s) is determined from the relationship:

$$Z_s = a \cdot \psi_r^2 + b \cdot \psi_r + c. \tag{14}$$

The equation can represent the complex impedance value using exponential and trigonometric notation:

$$\underline{Z}_s = Z_s \cdot e^{j\psi_r} = Z_s(cos\psi_r + jsin\psi_r). \tag{15}$$

3. Theoretical Determination of Method Errors

To identify errors in assessing fault-loop impedance using the proposed method, theoretical calculations were performed without accounting for the actual measurement circuit. The focus is solely on the intrinsic method error arising from the polynomial approximation, assuming perfect measurement conditions without instrument uncertainty, disturbances, or numerical noise.

The following assumptions (typical for low-voltage electrical installations) were made to determine the errors in the determination of short-circuit impedance values using the method proposed by the authors, based on the analysis of the RMS value of the line voltage of the circuit under test:

- mains voltage $\underline{E}_1 = \underline{E}_2 = \underline{E}_3 = 230$ V,
- actual fault-loop impedance $\underline{Z}_{sr} = 0.26 + 0.12j = 0.2864\ e^{j24.7751°}$ Ω.

The following values of the complex impedance were taken as the switched measuring branches of the measuring instrument in the following sequence: $\underline{Z}_{p1} = 50 + j1$ Ω, $\underline{Z}_{p2} = 0.5 + j50$ Ω, $\underline{Z}_{p3} = 35 + j35$ Ω, for which the moduli of the individual values are: $|Z_{p1}| = 50$ Ω, $|Z_{p2}| = 50.0025$ Ω, $|Z_{p3}| = 49.4975$ Ω, while the impedance phase angles are: $\psi_{p1} = 1.1458°$, $\psi_{p2} = 89.4271°$, $\psi_{p3} = 45°$.

The selection of three measurement impedances (Z_{p1}, Z_{p2}, Z_{p3}) was deliberate and aimed to ensure sufficient diversity in impedance phase angles to enable accurate approximation of the function with a second-degree polynomial. A second-degree polynomial was chosen because three measurement points are available, allowing a unique analytical solution with low computational complexity. The use of higher-order polynomials would require additional measurement impedances and a larger number of measurements, increasing both the duration of the procedure and the complexity of the measuring device.

The adopted values of the angles of individual impedances correspond approximately to 0°, 45°, and 90°, which represent typical boundary conditions for purely resistive (0°) and purely inductive (90°) circuits, as well as intermediate conditions for mixed resistive-inductive circuits (45°). This distribution of impedance angles ensures that the polynomial function used to determine the complex value of the fault-loop impedance is well-conditioned and minimizes numerical errors in coefficient estimation. The use of extreme phase angles enables reliable interpolation across the entire operating range from 0° to 90°.

The reference impedance angles were selected to provide wide and approximately uniform coverage of the investigated range from 0 to 90 degrees. Other combinations of impedance angles can be used, provided that they cover a sufficiently wide phase range and ensure non-collinearity of the approximation points. Nevertheless, simulation studies have shown that this configuration gives the smallest approximation error (below 1.1%) while maintaining high stability of the numerical solution. The value was determined from the maximum absolute approximation error obtained during numerical analysis of impedance angles over the range 0° to 90° with a 1° increment, as shown in Figures 3–6.

When the individual impedances are switched on, the following measurement currents will be forced to flow in the subsequent branches:

$$\begin{aligned} \underline{I}_{p1} &= \tfrac{\underline{E}_1}{\underline{Z}_s + \underline{Z}_{p1}} = 4.5739 - j0.1019 \ \text{ A}, \\ \underline{I}_{p2} &= \tfrac{\underline{E}_2}{\underline{Z}_s + \underline{Z}_{p2}} = 0.0696 - j4.5879 \ \text{ A}, \\ \underline{I}_{p3} &= \tfrac{\underline{E}_3}{\underline{Z}_s + \underline{Z}_{p3}} = 3.2745 - j3.2615 \ \text{ A}. \end{aligned} \tag{16}$$

These currents will cause a voltage drop in the subsequent measuring branches:

$$\begin{aligned} \underline{U}_{p1} &= \underline{I}_{p1} \cdot \underline{Z}_{p1} = 228.7985 - j0.5224 \ \text{ V}, \\ \underline{U}_{p2} &= \underline{I}_{p2} \cdot \underline{Z}_{p2} = 229.4314 - j1.1845 \ \text{ V}, \\ \underline{U}_{p3} &= \underline{I}_{p3} \cdot \underline{Z}_{p3} = 228.7573 - j0.4550 \ \text{ V}. \end{aligned} \tag{17}$$

which will be stored as consecutive RMS values of the measuring voltages:

$$\begin{aligned} U_{p1} &= 228.7991 \text{ V}, \\ U_{p2} &= 229.4344 \text{ V}, \\ U_{p3} &= 228.7577 \text{ V}. \end{aligned} \tag{18}$$

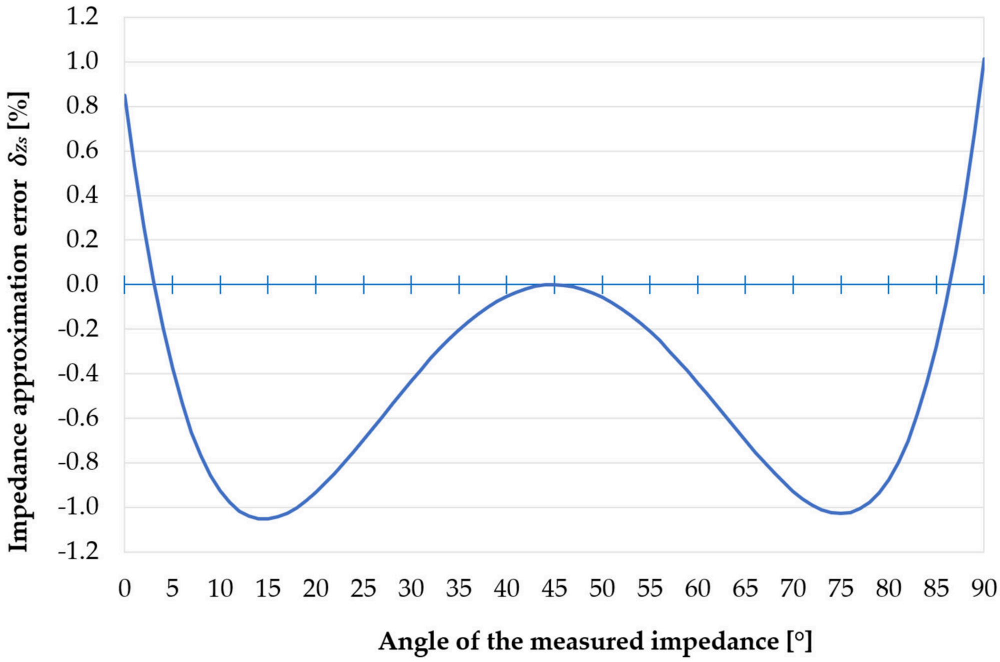

Figure 3. Approximation error of the fault-loop impedance modulus as a function of the actual impedance angle.

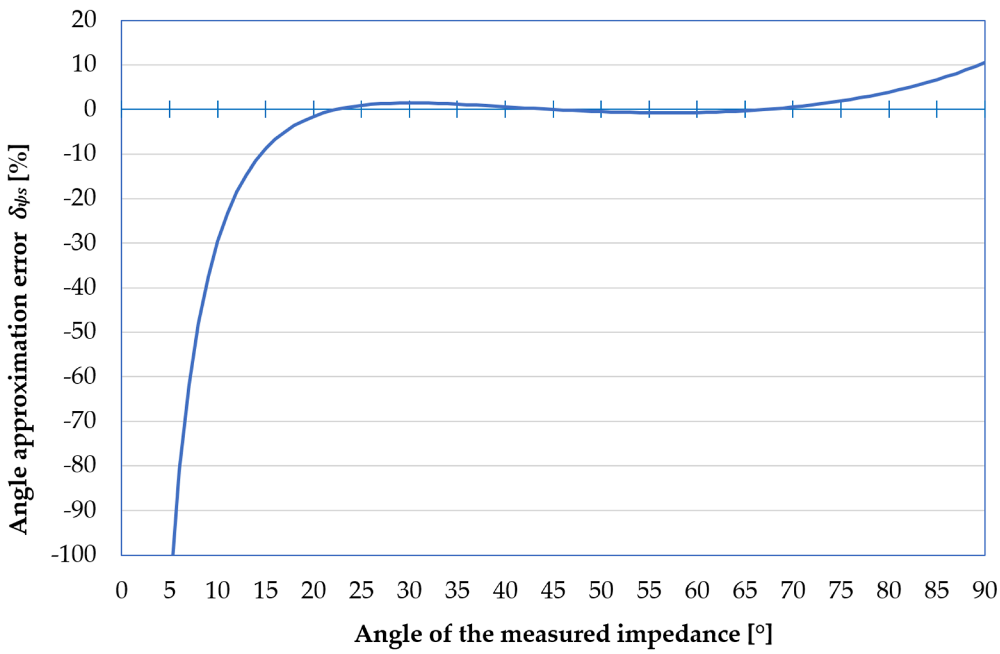

Figure 4. Approximation error of the fault-loop impedance angle as a function of the actual impedance angle.

Based on the known RMS, the test network voltages (values of E_1, E_2, E_3) and the values of the RMS measurement voltages (U_{p1}, U_{p2}, U_{p3}) obtained for the individual measurement branches, the fault-loop impedance moduli are determined:

$$\begin{aligned} Z_{s1} &= Z_{p1} \cdot \frac{(E_1 - U_{p1})}{U_{p1}} = 0.2625\ \ \Omega, \\ Z_{s2} &= Z_{p2} \cdot \frac{(E_2 - U_{p2})}{U_{p2}} = 0.1233\ \ \Omega, \\ Z_{s3} &= Z_{p3} \cdot \frac{(E_3 - U_{p3})}{U_{p3}} = 0.2688\ \ \Omega. \end{aligned} \tag{19}$$

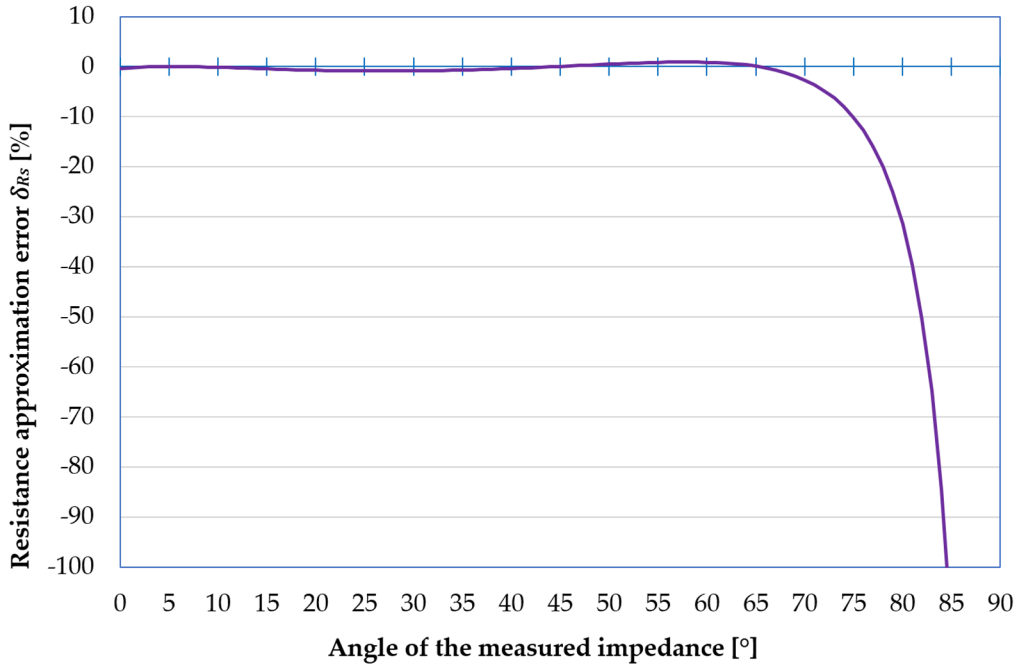

Figure 5. Approximation error of the resistive part of the fault-loop impedance as a function of the angle of the actual impedance.

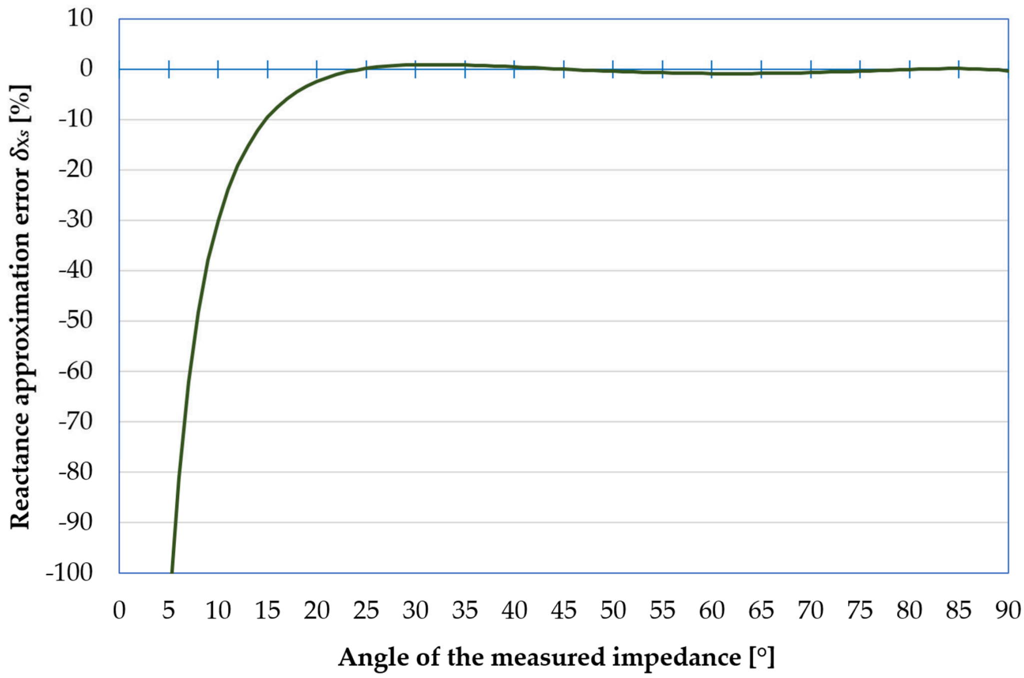

Figure 6. Approximation error of the reactance part of the fault-loop impedance as a function of the angle of the actual impedance.

The dependence of the value of the loop impedance modulus short-circuit (Z_{si}) as a function of the measurement impedance angle ($\psi_{(p)(i)}$) is approximated by a polynomial of the second degree (5). To determine the coefficients of the polynomial (a, b, c), a system of equations is formed:

$$\begin{cases} 1.1458^2 \cdot a + 1.1458 \cdot b + c = 0.2625 \\ 89.4271^2 \cdot a + 89.4271 \cdot b + c = 0.1233 \\ 45.0000^2 \cdot a + 45.0000 \cdot b + c = 0.2688 \end{cases} \tag{20}$$

Using the Cramer method system of equations to solve the above, the determinants of the matrix of coefficients of the system are obtained from equations (relations 7–10): $W = 1.7200 \cdot 10^5; W_a = -6.6632;\ W_b = 332.2688; W_c = 4.4774 \cdot 10^4$, and then the values of the coefficients of the polynomial (11): $a = -3.8740 \cdot 10^{-5}$; $b = 1.9318 \cdot 10^{-3}$; $c = 0.2603$.

From this, the value is determined as the fault-loop impedance angle (13): $\psi_s = 24.9330°$.

The value of the fault-loop impedance modulus (14) can then be determined:

$$Z_s = 0.2844\ \Omega. \tag{21}$$

Thus, the determined (using the developed method) by the authors' complex value of the fault-loop impedance ($\underline{Z}_s$) for the circuit under test, low-voltage, is:

$$\underline{Z}_s = 0.2844 \cdot e^{j24.9330°} = 0.2579 + j0.1199\ \Omega. \tag{22}$$

It follows that the resistance (R_s) and reactance (X_s) values of the fault-loop are as follows:

$$R_s = 0.2579\ \Omega \quad X_s = 0.1199\ \Omega. \tag{23}$$

For this example, the approximation errors for the individual components of the fault-loop impedance are, respectively [21]:

- the error of approximation of the fault-loop impedance modulus:

$$\delta_{Zs} = \frac{Z_s - Z_{sr}}{Z_{sr}} \cdot 100\% = -0.6836\%, \tag{24}$$

- the error of approximation of the fault-loop impedance angle:

$$\delta_{\psi s} = \frac{\psi_s - \psi_{sr}}{\psi_{sr}} \cdot 100\% = 0.6374\%, \tag{25}$$

- the error of approximation of fault-loop resistance:

$$\delta_{Rs} = \frac{R_s - R_{sr}}{R_{sr}} \cdot 100\% = -0.8103\%, \tag{26}$$

- the error of approximation of the fault-loop reactance:

$$\delta_{Xs} = \frac{X_s - X_{sr}}{X_{sr}} \cdot 100\% = -0.0909\%. \tag{27}$$

To evaluate the intrinsic approximation error of the proposed method, calculations were performed over the entire investigated range of the actual impedance angle. The calculations were performed step-by-step using Equations (4)–(14) with SMath Studio 64-bit (ver. 1.4.0.9654) software. The calculations assumed a constant value of the measured fault-loop impedance Z_s = 0.17 Ω and a variable impedance angle ψ_r from 0° to 90° in 1° increments. For each ψ_r value, the values of Zs, ψs, Rs, and Xs were first determined, followed by their approximation errors δ_{Zs}, $\delta_{\psi s}$, δ_{Rs}, and δ_{Xs}. The results were exported from SMath Studio into a Microsoft Excel spreadsheet, where graphs of each error versus the measured impedance angle ψ_r were plotted. This approach ensured the consistency and repeatability of the resulting characteristics. The graphs of the approximation errors are shown in Figures 3–6.

As shown in Figure 3, the approximation error of the fault-loop impedance modulus does not have a constant sign and does not exceed 1.1 percent over the entire range of the actual impedance angle. The largest errors are observed for impedance angles close to 0, 15, 75, and 90 degrees, whereas the error is negligible for impedance angles of 3, 45, and 87 degrees.

Figure 4 shows the dependence of the error of the impedance angle approximation on the angle of the actual impedance. It is worth noting that for angles between 20 and 70 degrees, the error is close to 0. Nevertheless, beyond this range, the error value increases significantly to reach 100% for angles of 5 degrees.

The approximation error of the fault-loop resistance as a function of the angle of the actual impedance is shown in Figure 5. As it can be seen from the waveform presented there, the proposed method by the authors works well for determining the resistance of systems at impedance angles smaller than 70 degrees (then the approximation error is close to 0). The error increases for larger angles, which is related to a larger share of reactance in the system under test. The situation is reversed when determining the reactance part of the fault-loop impedance-Figure 6. High accuracy is obtained for fault-loop impedance angles greater than 20 degrees. In other cases, due to the significant share of the resistive part in the system, the approximation error reaches up to 100 percent.

The large relative errors of the resistance or reactance component near 0° and 90° result mainly from the fact that one of these components approaches zero. Therefore, even a small absolute estimation error may correspond to a very large relative error. This effect does not imply an equally large error in the impedance modulus; however, it indicates that the decomposition into resistance and reactance becomes poorly conditioned near the boundaries. Consequently, the complete complex impedance estimate should be treated as reliable primarily within the central phase-angle range. A solution is accepted only when $a < 0$ and $0^\circ \leq -b/(2a) \leq 90^\circ$; otherwise, it is rejected as physically invalid. Adaptive selection of the reference angles and the use of additional measurement branches will be investigated in future work.

In order to comprehensively assess the effectiveness of the method proposed by the authors, it was compared with one of the most commonly used direct methods–the classic voltage drop measurement method, also known as the artificial short-circuit method [18,20,21]. This method involves measuring the voltage before and after connecting a load with a known impedance, and the fault-loop impedance is calculated based on the voltage difference [20]. Despite its popularity, this method has significant limitations. As indicated in [7,23], the accuracy of the measurement depends on the value of the measured impedance and the nature of the operating loads in the circuit under test. In particular, with a large reactive component or low phase angles, measurement errors can be significant. In addition, the presence of harmonic disturbances and variable network conditions negatively affects the stability of the results [21,24].

The errors of both methods for different impedance values and phase angles, assuming typical conditions for low-voltage installations, are shown in Table 1. The classical voltage-drop method and the proposed method were evaluated under the same conditions used in References [7,18,20,21,23].

The comparison with modern grid-impedance estimation techniques is limited to the discussion of their application scope because these methods differ substantially from the proposed approach in terms of measurement objective, required signals, and hardware structure.

The error values of the classical method were calculated using the assumptions and calculation procedure reported in References [7,18,20,21,23], whereas the errors of the proposed method were determined for exactly the same test cases using Equations (4)–(14).

Table 1. Comparison of the classical voltage-drop method and the proposed method under the same network and measurement conditions adopted in References [7,18,20,21,23].

Impedance Modulus Z_{sr} [Ω]	Impedance Angle ψ_{sr} [°]	The Error of the Classical Method δ_{Zs} [%]	Error in the Developed Method δ_{Zs} [%]
0.17	28	±2.3	−0.53
0.20	45	±3.1	−0.12
0.25	70	±4.5	−0.89
0.15	5	±6.8	+1.36
0.18	87	±5.2	+0.02

Under the common theoretical conditions adopted in Table 1, the proposed method produced lower impedance-magnitude errors than the classical voltage-drop method for the investigated cases. However, this result is limited to the assumptions of the adopted mathematical model and should not be interpreted as experimental evidence of the general superiority of the proposed method or its immunity to network disturbances.

The use of unloaded voltage measurements before and after each loading interval is intended to reduce sensitivity to slowly varying operating loads, provided that the voltage-stationarity criterion is satisfied. The influence of rapid load variations, measurement noise, switching transients, and other network disturbances requires experimental verification. The influence of harmonic distortion will be investigated in future work.

4. Measurement Uncertainty Discussion

Uncertainty measurements of results are a key element of modern metrology, where the definition of measurement error has been replaced by measurement result uncertainty. The basis for uncertainty analysis is the international guide GUM (Guide to the Expression of Uncertainty in Measurement), developed by JCGM [29–32]. This document defines the principles for identifying and evaluating the components of uncertainty. There are two basic types: Type A uncertainty, determined by statistical methods based on repeated measurements, and Type B uncertainty, determined from other available information such as instrument data, calibration results, or experience. Uncertainty defines the range of values that can reliably be attributed to the measured quantity, giving the result a qualitative and informational dimension. Considering it allows for comparing results, assessing compliance with requirements, and ensuring metrological conformity. Estimating measurement uncertainty is especially important in complex measurements, such as the impedance measurements presented here, where many factors can significantly influence the final measurement result. Below, an example approach to determining measurement uncertainties for the presented method will be shown. In a real measurement device system, in order to simplify the analysis of the measurement result, a different approach is proposed, in which the resolution and accuracy of the instrument will be specified.

The presented method is based on determining the complex value of the fault-loop impedance (2) and (3) by triple loading the network with measurement impedances (4) with known magnitudes and phase angles. For each load, the effective voltage under load (18) is measured. Based on the three sets of results (19), a second-degree polynomial approximation (20) is performed, whose maximum corresponds to the actual value of the magnitude and phase angle of the fault-loop impedance.

For the presented twelve critical values (Table 2) and the uncertainty in determining coefficients a, b, c, it is necessary to consider the procedure for calculating the final measurement result according to the process outlined below. Firstly, the measurement device or ADC (Analog-to-Digital Converter) error limit must be determined. In the case of voltage measurement using an ADC, the method of estimating uncertainty differs from the classical approach used for analog voltmeters. Instead of using an accuracy class expressed as a percentage of the measurement range, the uncertainty is determined based on the physical and operational parameters of the converter. According to the manufacturer's documentation for a given converter, we consider the following: quantization (LSB, Least Significant Bit), resulting from the limited resolution of the converter; measurement noise causing random fluctuations in readings; and inaccuracies specified by the manufacturer, including nonlinearity, temperature drift, or calibration errors. For example, quantization, defined by the smallest significant bit (LSB), generates a standard uncertainty according to the following relation:

$$u_{LSB} = \frac{LSB}{\sqrt{12}}, \tag{28}$$

Table 2. Uncertainty components important in estimating the accuracy of measurement results.

Uncertainty Components	Character	Uncertainty Source
E_1, E_2, E_3	Three measurements	Voltmeter (ADC) inaccuracy
U_{p1}, U_{p2}, U_{p3}	Three measurements	Voltmeter (ADC) inaccuracy
$\lvert Z_{p1} \rvert, \lvert Z_{p2} \rvert, \lvert Z_{p3} \rvert$	Threefold use of the reference standard	Tolerance of reference elements
$\psi_{p1}, \psi_{p2}, \psi_{p3}$	Threefold use of the reference standard	Reference impedance angle error
a, b, c	Uncertainty coefficients calculation	Binomial method, nonlinear character

In the ±½ LSB interval, a uniform distribution is assumed according to GUM guidelines, which mandate the use of a rectangular distribution with equal probability within the quantization step. When nonlinearity, temperature drift, and calibration errors are considered by the ADC manufacturer as maximum errors, we convert these to standard uncertainty by assuming a triangular distribution u_{Btri} or a rectangular distribution u_{Brect}, depending on the degree of confidence in the error distribution, according to the formulas presented below:

$$u_{Btri} = \frac{\Delta_{max}}{\sqrt{6}}, \qquad u_{Brect} = \frac{\Delta_{max}}{\sqrt{3}}. \tag{29}$$

Ultimately, according to the manufacturer's documentation for this particular case, the maximum measurement error can be assumed to be:

$$ADC_e = \pm 1 \text{ mV}. \tag{30}$$

Considering the maximum error limit ADC_e, it is generally assumed that the true voltage value can be anywhere within the range of $\pm ADC_e$ with equal probability. This implies the use of a rectangular (uniform) distribution. In this case, the standard uncertainty of the voltage is determined separately for the measured line voltage E_i and the voltage with the reference load connected U_i using the formula:

$$u_B(E_i) = \frac{ADC_e}{\sqrt{3}}, u_B(U_i) = \frac{ADC_e}{\sqrt{3}}. \tag{31}$$

Since the E_i and U_i voltages are measured multiple times, it is necessary to consider Type A uncertainty, which is derived from statistical analysis of repeated measurements. For each of the three load conditions, a series of measurements is conducted, and the Type A uncertainty is represented by the sample standard deviation, expressed as the standard deviation of the mean using the following formulas:

$$u_A(E_i) = \sqrt{\frac{\sum_{i=1}^{n}\left(E_i - \overline{E}\right)^2}{n(n-1)}}, u_A(U_i) = \sqrt{\frac{\sum_{i=1}^{n}\left(U_i - \overline{U}\right)^2}{n(n-1)}}, \tag{32}$$

Further on, we determine the total uncertainty:

$$u(E_i) = \sqrt{u_A(E_i)^2 + u_B(E_i)^2}, u(U_i) = \sqrt{u_A(U_i)^2 + u_B(U_i)^2}, \tag{33}$$

where i—denotes the i-th measurement, n—denotes the number of measurements, E_i and U_i denote the voltage values in the respective measurements, and $\overline{E}$ and $\overline{U}$ denote the mean values of the measurements.

It is worth noting that the above values reflect random fluctuations resulting from thermal noise, external interference, and variations in the system operating conditions, and serve as a direct measure of the repeatability of the measurement sequence.

Another factor affecting the accuracy of the method is the determination of the impedance modulus and phase angle of the reference impedances connected to the circuit. The manufacturer provides relevant information regarding these parameters with the reference impedances. Nevertheless, these parameters can be determined experimentally using a conventional approach or by conducting tests with an RLC measuring bridge. The RLC bridge measurement yields the actual values of the modulus Z_{pi} and the phase angle ψ_{pi}, which are then used as reference values in subsequent calculations. The use of reference impedance measurements allows for a significant reduction in the overall uncertainty of the method, particularly by reducing the dominant Type B component. Based on the manufacturer's information, this uncertainty can be described using data on the limit errors of the impedance module and the phase angle of the reference impedance, applying a rectangular distribution in accordance with the recommendations of the GUM guide:

$$u_B(Z_{pi}) = \frac{\Delta Z_{pi}}{\sqrt{3}}, \qquad u_B(\psi_{pi}) = \frac{\Delta\psi_{pi}}{\sqrt{3}}, \tag{34}$$

where ΔZ_{pi} and $\Delta\psi_{pi}$ denote the uncertainty limits of the calibrated magnitude and phase angle of the i-th reference impedance, respectively.

The reference impedances are not assumed to be perfectly known. Their calibrated moduli Z_{pi} and phase angles ψ_{pi} are treated as input quantities with Type B standard uncertainties. These uncertainties may include component tolerances, calibration errors, temperature drift, and long-term aging. In a practical implementation, the corresponding uncertainty distributions should be determined experimentally and included in the Monte Carlo propagation model. Since the present study is theoretical and no long-term drift data for a physical prototype is available, arbitrary numerical drift values were not introduced. This limitation will be addressed during the experimental validation of the measuring device.

It is worth noting that the final measured quantity is the complex value of the fault-loop impedance Z_s, determined indirectly based on voltage measurements for each branch containing the corresponding three reference impedances, in accordance with Equation (3). On this basis, the uncertainty propagation should therefore be determined according to the following relationship:

$$u(Z_{si}) = \sqrt{\left(\frac{\partial Z_{si}}{\partial E_i}u(E_i)\right)^2 + \left(\frac{\partial Z_{si}}{\partial U_{pi}}u(U_{pi})\right)^2 + \left(\frac{\partial Z_{si}}{\partial Z_{pi}}u(Z_{pi})\right)^2 + \left(\frac{\partial Z_{si}}{\partial \psi_{pi}}u(\psi_{pi})\right)^2}. \tag{35}$$

where the variable i = 1, 2, 3, means that we must apply the above equation three times for each reference impedance connected to the circuit. In the present analysis, correlations between input quantities were assumed negligible. This assumption simplifies the uncertainty propagation model and is acceptable for the theoretical assessment presented in this work. In summary, the entire measurement cycle up to this point must be repeated three times for each of the circuit branches being connected, i.e.:

- for branch 1 of the measured electrical circuit:

$$u(Z_{s1}) = f(E_1, U_{p1}, Z_{p1}, \psi_{p1}), \tag{36}$$

- for branch 2 of the measured electrical circuit:

$$u(Z_{s2}) = f(E_2, U_{p2}, Z_{p2}, \psi_{p2}), \tag{37}$$

- for branch 3 of the measured electrical circuit:

$$u(Z_{s3}) = f(E_3, U_{p3}, Z_{p3}, \psi_{p3}). \tag{38}$$

This gives us three measurement results with the corresponding uncertainties:

$$Z_{s1} \pm u(Z_{s1}),\ Z_{s2} \pm u(Z_{s2}),\ Z_{s3} \pm u(Z_{s3}), \tag{39}$$

which will be used to determine the coefficients a, b, and c:

$$(a,\ b,\ c) = f(Z_{s1},\ Z_{s2},\ Z_{s3},\ \psi_{p1}\ \psi_{p2},\ \psi_{p3}). \tag{40}$$

The three obtained impedance values, Z_{s1}, Z_{s2}, $Z_{s3,}$ along with their uncertainties, serve as input points for the polynomial approximation procedure. Each of these points is associated with an uncertainty resulting from the propagation of measurement errors in voltage and the uncertainties of the reference impedances. Therefore, the coefficients of the second-degree polynomial a, b, and c, determined based on these points, are also uncertain quantities. The uncertainty of the final impedance Z_s results from propagating the uncertainties of the three measurement points through the approximation model. Due to the nonlinear nature of the relationship, this propagation is most conveniently performed using the Monte Carlo method, which involves repeatedly sampling Z_{si} values according to their uncertainty distributions, determining the polynomial coefficients, and calculating the final impedance value based on Formulas (13) and (14). Of course, after completing the entire procedure, the expanded uncertainty should be calculated by multiplying the result by the coverage factor k = 2 for a 95% confidence level.

Example Calculation of Uncertainty Components

For the input data presented in Section 3 (Theoretical determination of method errors), the impedance modules of the standards were first calculated (Figure 7), and then the fault-loop impedance was determined indirectly according to Equation (19). Next, by determining the coefficients of the principal matrix, we determine the coefficients of the polynomial (21).

The next step is to determine the nominal impedance Z_s (22), which is a deterministic value calculated using an analytical equation. The impedance value in this form does not have an uncertainty measure, which we will determine using the Monte Carlo method [33]. Up to this point, the calculations are fully consistent with those presented in Section 3. Only in the subsequent steps will the individual components of uncertainty be calculated, which determine the expected accuracy of the method.

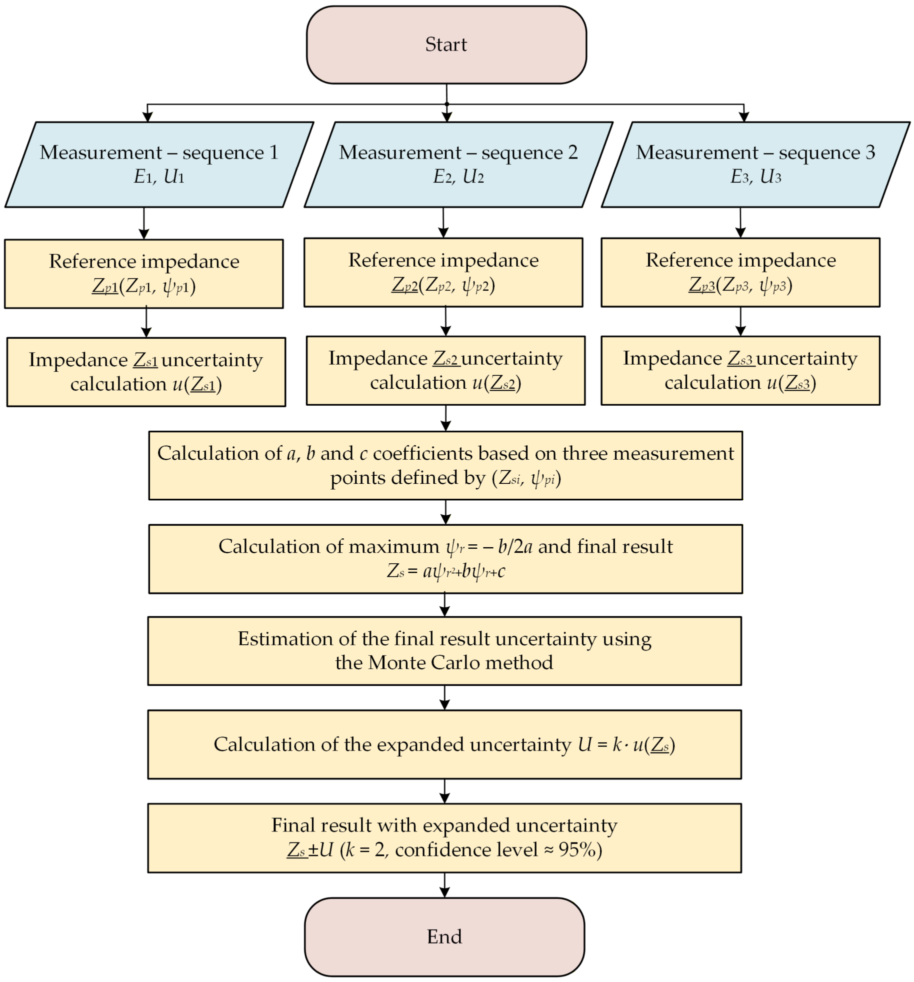

Figure 7. General algorithm for determining the measurement uncertainty of the presented method.

The presented Monte Carlo analysis is intended only to illustrate the propagation of voltage-measurement uncertainty through the nonlinear calculation procedure. It does not constitute a complete metrological validation of a practical instrument. Numerical uncertainty limits for the reference-impedance magnitudes and phase angles were not introduced because no calibrated prototype or experimentally determined temperature- and aging-drift data are currently available. Introducing arbitrary values would not provide a reliable assessment of practical measurement uncertainty. A complete Monte Carlo model including these effects will be developed during future experimental validation.

For this illustrative Monte Carlo analysis, the unloaded voltages E_i and the loaded voltages U_{pi} were treated as independent input quantities. Each voltage value was sampled from a uniform distribution centered at its nominal value with a half-width of $\Delta U = 0.015$ V. This value represents the assumed uncertainty limit of the voltage measurement subsystem and was selected to illustrate uncertainty propagation through the nonlinear computation algorithm while remaining representative of a practical high-resolution voltage measurement system. Under the assumption of a uniform distribution, the corresponding standard uncertainty was taken as $u(U) = \Delta U/\sqrt{3}$. The voltage measurements were assumed to be statistically independent.

It is important to note that for each Monte Carlo trial, random values of E_i and U_{pi} were generated first. The corresponding impedance magnitudes Z_{s1}, Z_{s2} and Z_{s3} were then calculated using Equation (19). Next, the coefficients a, b and c of the second-degree polynomial were determined, followed by the calculation of the fault-loop impedance modulus Z_s and the corresponding impedance angle according to Equations (13) and (14).

Moreover, solutions for which $a \geq 0$ or for which the calculated maximum occurred outside the physical range from 0° to 90° were rejected as physically invalid. The simulation was repeated 100,000 times, and the resulting distribution of impedance values was used to determine the mean value, standard uncertainty, and expanded uncertainty. As a result of this simulation, we obtained a dataset presented as a histogram (Figure 8) in the following form:

$$\begin{aligned} Z_s^{(1)} &= 0.283 \\ Z_s^{(2)} &= 0.287 \\ Z_s^{(3)} &= 0.281 \\ &\dots \\ Z_s^{(100000)} &= 0.282 \end{aligned} \tag{41}$$

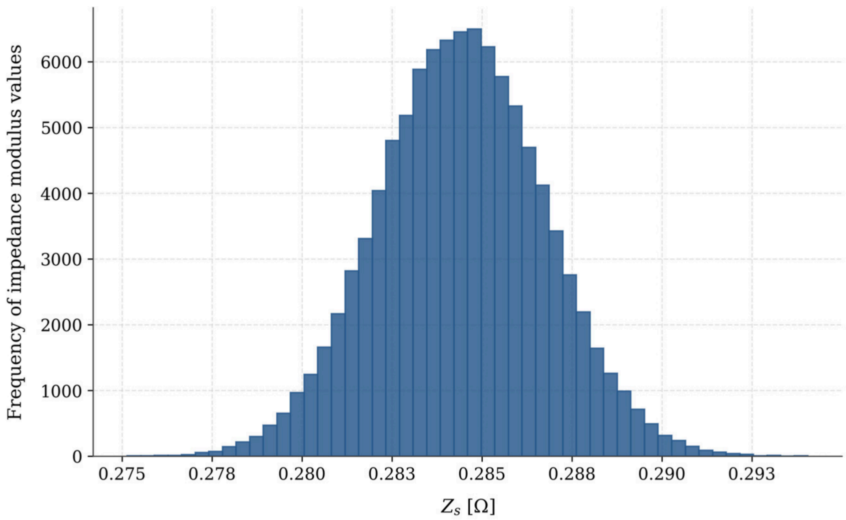

Figure 8. Histogram of fault-loop impedance values obtained from 100,000 Monte Carlo simulations with independently sampled unloaded and loaded voltages (uniform distribution, half-width = 0.015 V, seed = 50).

Next, we determine the mean value and the standard deviation of the average impedance modules obtained. This way, we obtain a measure of uncertainty. Then, we calculate the expanded uncertainty and record the final result:

$$Z_s = (0.2844 \pm 0.0046)\ \Omega,\ k = 2,\ p \approx 95\%. \tag{42}$$

Based on this, the basic measure of the method accuracy can be determined as the relative standard uncertainty, defined by the following relation:

$$\delta = \frac{u(Z_s)}{Z_s} \cdot 100\%. \tag{43}$$

which, after substituting numerical data, provides a result with the appropriate relative accuracy and relative uncertainty at a 95% confidence level:

$$\delta = \frac{0.0023}{0.2844} \cdot 100\% \approx 0.8\%, \text{ or for } p \approx 95\%\ \delta_{95\%} \approx 1.6\%. \tag{44}$$

5. Conclusions

This paper presents a new method for determining the complex value of the fault-loop impedance, based solely on measurements of effective voltage values and polynomial approximation. The proposed method does not require direct measurement of the phase angle and, under the adopted theoretical assumptions and voltage-stationarity criterion, may reduce sensitivity to slowly varying operating loads. The results of theoretical analyses indicate that the approximation error of the impedance magnitude does not exceed 1.1% across the entire range of impedance phase angles. The lowest intrinsic approximation errors were obtained within the range from 20° to 70°, which corresponds to typical operating conditions of low-voltage installations. The method also allows for reliable determination of both the resistive and reactive components within this range.

An important contribution of this work is the inclusion of an uncertainty analysis based on the guidelines of the GUM (Guide to the Expression of Uncertainty in Measurement). Using the Monte Carlo method to propagate uncertainty provides a clear illustration of how the assumed voltage-measurement uncertainty spreads through the analysis. The uncertainties of the reference impedances were discussed within the uncertainty model but were not numerically included in the illustrative Monte Carlo simulation. The simulation results indicate a relative expanded uncertainty of approximately 1.6% ($k = 2$, $p \approx 95\%$) under the adopted assumptions. The presented uncertainty calculation is illustrative and is limited to the assumed voltage-measurement uncertainty. A complete uncertainty budget requires experimentally determined calibration, temperature-drift, and aging data for the reference impedances. Additionally, the proposed approach offers significant practical advantages, such as reduced measurement current requirements, simplified measurement system design, and the possibility of fully automating the measurement process. Electronically controlled reference branches and an automated measurement sequence suggest that this solution could be used in a digital measuring device; however, its accuracy, thermal properties, susceptibility to interference, and safety must be verified experimentally. However, near 0° and 90°, the phase angle and the smaller impedance component become poorly conditioned because one of the components approaches zero. Consequently, even a small absolute error may produce a very large relative error in the resistance or reactance, whereas the impedance modulus may still be estimated with a relatively low error. Therefore, the complete complex impedance estimate is most reliable within the central phase-angle range. Further research will focus on optimizing the reference-angle selection and investigating adaptive or additional measurement branches to improve the accuracy near the boundaries.

In summary, the proposed method constitutes a promising theoretical approach with practical potential for determining the complex fault-loop impedance in low-voltage electrical installations. Its measurement accuracy, repeatability, thermal performance, disturbance sensitivity, and practical usability require experimental validation using a physical prototype. Although the proposed method requires three sequential measurements, the procedure can be fully automated and implemented using electronically controlled switching circuits. The influence of the additional measurement steps on the total measurement time and the usability of a practical instrument will be evaluated during prototype testing. It is also worth mentioning that the present analysis assumes sinusoidal steady-state conditions. The influence of harmonic distortion and non-sinusoidal waveforms was not considered and should be investigated in future studies. Additionally, future research will focus not only on improving the approximation model but also on reducing estimation errors observed at extreme impedance angles (close to 0° and 90°). Potential solutions include optimization of the phase angles of the reference impedances, adaptive selection of measurement branches, and the application of alternative approximation techniques better suited to boundary conditions. The increased error observed near 0° and 90° is primarily related to the reduced sensitivity of the polynomial approximation when one component of the impedance vector (resistive or reactive) becomes dominant.

6. Patents

On the basis of the research described in the article, a patent was obtained, granted by the Patent Office of the Republic of Poland, no. PL 233 169 B1, Bialystok University of Technology, Bialystok, Poland: Method and system for measuring short-circuit loop impedance [28]. The patent covers the measurement concept, switching sequence, and measurement system architecture. The mathematical analysis, uncertainty evaluation, and theoretical performance assessment presented in this paper are fully disclosed for scientific purposes.

Author Contributions: Conceptualization, G.H. and Z.S.; methodology, G.H. and W.W.; software, G.H.; validation, G.H.; formal analysis, G.H., Z.S. and W.W.; investigation, G.H. and W.W.; resources, G.H. and Z.S.; data curation, G.H. and Z.S.; writing—original draft preparation, G.H., W.W. and Z.S.; writing—review and editing, G.H., Z.S. and W.W.; visualization, G.H. and W.W.; supervision, W.W.; project administration, G.H. and Z.S.; funding acquisition, W.W. All authors have read and agreed to the published version of the manuscript.

Funding: The work was supported by scientific work WZ/WE-IA/7/2026 conducted in the Department of Electrotechnics, Power Electronics and Electrical Power Engineering at Bialystok University of Technology.

Data Availability Statement: The raw data supporting the conclusions of this article will be made available by the authors on request.

Conflicts of Interest: The authors declare no conflicts of interest.

References

1. Katarzyński, J.; Fault, M. Loop Impedance Measurement in Circuits Fed by UPS and Principle of Safety Protection. *Sustainability* **2020**, *12*, 10126. [CrossRef]
2. Aigner, M.; Schmautzer, E.; Sigl, C. Fault Loop Impedance Determination in Low-Voltage Distribution Systems with Non-Linear Sources. In *Proceedings of the IEEE PES ISGT Europe*; IEEE: Piscataway, NJ, USA, 2013; pp. 1–5.
3. Liu, H.; Mitolo, M.; Qiu, J. Ground-Fault Loop Impedance Calculations in Low-Voltage Single-Phase Systems. *IEEE Trans. Ind. Appl.* **2014**, *50*, 1331–1337. [CrossRef]
4. Neamt, L.; Balan, H.; Hotea, A. Considerations about Fault Loop Impedance Measurement in TN Low-Voltage Network. In *Proceedings of the 8th International Conference on Modern Power Systems (MPS)*; IEEE: Piscataway, NJ, USA, 2019; pp. 1–4.
5. Low Voltage Electrical Installations—Part 6: Verification IEC 60364-6:2016. Available online: https://www.en-standard.eu/iec-60364-6-2016-low-voltage-electrical-installations-part-6-verification/?srsltid=AfmBOoqMrL5lXSiVmsZXEirnY86US7gySSXAwSUW7nbyZRTVnfCXYNF6 (accessed on 6 June 2026).
6. Low Voltage Electrical Installations—Part 4-41: Protection for Safety—Protection Against Electric Shock IEC 60364-4-41:2005. Available online: https://www.en-standard.eu/iec-60364-4-41-2005-amd1-2017-csv-low-voltage-electrical-installations-part-4-41-protection-for-safety-protection-against-electric-shock/?gad_source=1&gad_campaignid=23589929400&gbraid=0AAAAAD6CNv-OKC2uL9Bl5ymgRpuOfQp1h&gclid=Cj0KCQjwio_RBhDMARIsAJPveNOOvFSLV6Si0z-3pqXSoR4RPxJRyv69QvTjbdVRkfIb2u8eWvZ_oGAaArP2EALw_wcB (accessed on 6 June 2026).
7. Czapp, S. Fault Loop Impedance Measurement in Low Voltage Networks with Residual Current Devices. *Electron. Electr. Eng.* **2012**, *122*, 109–112. [CrossRef]
8. Neamt, L.; Neamt, A.; Chiver, O. Improved Procedure for Earth Fault Loop Impedance Measurement in TN Low-Voltage Networks. *Energies* **2021**, *14*, 205. [CrossRef]
9. Zhong, P.; Sun, J.; Qu, L.; Yu, P.; Zha, X. An Improved PRBS-Injection-Based Grid Impedance Measurement Method Considering Nonideal Grid Conditions. *IEEE Trans. Ind. Electron.* **2023**, *70*, 6452–6456. [CrossRef]
10. Sun, J. Impedance-Based Stability Criterion for Grid-Connected Inverters. *IEEE Trans. Power Electron.* **2011**, *26*, 3075–3078. [CrossRef]
11. Gurumurthy, S.K.; Uhl, R.; Pitz, M.; Ponci, F.; Monti, A. Non-Invasive Wideband-Frequency Grid Impedance Measurement Device. In *Proceedings of the 2019 IEEE 10th International Workshop on Applied Measurements for Power Systems (AMPS)*; IEEE: Piscataway, NJ, USA, 2019; pp. 1–6.
12. Liserre, M.; Teodorescu, R.; Blaabjerg, F. Stability of Grid-Connected PV Inverters with Large Grid Impedance Variation. In *Proceedings of the 2004 IEEE 35th Annual Power Electronics Specialists Conference*; IEEE: Piscataway, NJ, USA, 2004; pp. 4773–4779.

13. Kaspirek, M.; Mezera, D. Voltage Quality Parameters in LV Distribution Grids in Dependence on Short Circuit Impedance. In *Proceedings of the 22nd Int. Conf. Electricity Distribution*; IET: Stevenage, UK, 2013.
14. Palethorpe, B.; Sumner, M.; Thomas, D.W.P. Power System Impedance Measurement Using a Power Electronic Converter. In *Proceedings of the Ninth International Conference on Harmonics and Quality of Power*; IEEE: Piscataway, NJ, USA, 2000; pp. 208–213. [CrossRef]
15. Chiulan, T.; Pantelimon, B. A Practical Example of Power Transformer Unit Winding Condition Assessment by Means of Short-Circuit Impedance Measurement. In *Proceedings of the IEEE PowerTech*; IEEE: Piscataway, NJ, USA, 2009.
16. Venikar, P.A.; Ballal, M.S.; Umre, B.S.; Suryawanshi, H.M. Sensitive Incipient Interturn Fault Detection Algorithm for Power Transformers. *IET Electr. Power Appl.* **2016**, *10*, 858–868. [CrossRef]
17. Do, T.T.; Jordan, M.; Langkowski, H.; Schulz, D. Novel Grid Impedance Measurement Setups in Electrical Power Systems. In *Proceedings of the 2016 IEEE International Workshop on Applied Measurements for Power Systems (AMPS)*; IEEE: Piscataway, NJ, USA, 2016; pp. 1–6.
18. Mitolo, M.; Bajzek, T.J. New Generation Tester to Assess the Electrical Safety in Low-Voltage Distribution Systems. *IEEE Trans. Ind. Appl.* **2019**, *55*, 106–110. [CrossRef]
19. Davis, P.; Wright, P.S. Measurement of Grid Impedance at Harmonic Frequencies. In *Proceedings of the 2018 Conference on Precision Electromagnetic Measurements (CPEM)*; IEEE: Piscataway, NJ, USA, 2018; pp. 1–2.
20. Czapp, S.; Borowski, K. Evaluation of Applicability of Classic Methods of a Fault Loop Impedance Measurement to Circuits with Residual Current Devices. *Acta Energ.* **2016**, *28*, 45–52. [CrossRef]
21. Czapp, S.; Borowski, K. Verification of Safety in Low-Voltage Power Systems without Nuisance Tripping of Residual Current Devices. *Electr. Power Syst. Res.* **2019**, *172*, 260–268. [CrossRef]
22. Mitolo, M. *Electrical Safety of Low-Voltage Systems*; The McGraw-Hill: New York, NY, USA, 2009; ISBN 9780071508186.
23. Czapp, S.; Guzinski, J. Electric Shock Hazard in Circuits with Variable-Speed Drives. *Bull. Pol. Acad. Sci. Tech. Sci.* **2018**, *66*, 361–372. [CrossRef] [PubMed]
24. Czapp, S.; Borowski, K.; Dobrzyński, K.; Klucznik, J.; Lubośny, Z. A New Method of Fault Loop Resistance Measurement in Low Voltage Systems with Residual Current Devices. In *Proceedings of the International Lubosny Conference "PowerTech 2015"*; IEEE: Piscataway, NJ, USA, 2015; pp. 1–6.
25. Roskosz, R. Method and System for Digital Measurement of Short Circuit Loop Impedance 1989. *IEEE Trans. Power Deliv.* **1991**, *6*, 546–549.
26. Roskosz, R.; Czapp, S.; Galla, S.; Golijanek, A. Method and System for Measuring Orthogonal Components and Modulus of Short Circuit Loop Impedance Vector. Polish Patent PL 198002 B1, 30 June 2008.
27. Roskosz, R.; Jakubiuk, K.; Swędrowski, L.; Świsulski, D.; Wołoszyk, M.; Ziółko, M. Method and System for Measuring Short-Circuit Loop Impedance in Low-Voltage Networks with Switched Differential Current. Polish Patent PL 223241 B1, 31 August 2016.
28. Hołdyński, G.; Skibko, Z. Method and System for Measuring Short Circuit Loop Impedance. Polish Patent PL 233169 B1, 24 May 2019.
29. Lequin, R.M. Guide to the Expression of Uncertainty of Measurement: Point/Counterpoint. *Clin. Chem.* **2004**, *50*, 977–978. [CrossRef] [PubMed]
30. BIPM; IEC; IFCC; ILAC; ISO; IUPAC; IUPAP. *OIML Guide to the Expression of Uncertainty in Measurement—Part 1: Introduction*; Joint Committee for Guides in Metrology (JCGM): Sèvres, France, 2008.
31. BIPM; IEC; IFCC; ILAC; ISO; IUPAC; IUPAP. *OIML Évaluation Des Données de Mesure—Guide Pour l'Expression de l'Incertitude de Mesure*; Joint Committee for Guides in Metrology (JCGM): Sèvres, France, 2008.
32. BIPM; IEC; IFCC; ILAC; ISO; IUPAC; IUPAP. *OIML Guide to the Expression of Uncertainty in Measurement—Part 6: Developing and Using Measurement Models*; Joint Committee for Guides in Metrology (JCGM): Sèvres, France, 2020.
33. BIPM; IEC; IFCC; ILAC; ISO; IUPAC; IUPAP. *OIML Evaluation of Measurement Data—Supplement 1 to the "Guide to the Expression of Uncertainty in Measurement"—Propagation of Distributions Using a Monte Carlo Method*; Joint Committee for Guides in Metrology (JCGM): Sèvres, France, 2008.